



Vibrational dynamics and band structure of methyl-terminated Ge(111)

Zachary M. Hund, Kevin J. Nihill, Davide Campi, Keith T. Wong, Nathan S. Lewis, M. Bernasconi, G. Benedek, and S. J. Sibener

Citation: *The Journal of Chemical Physics* **143**, 124705 (2015); doi: 10.1063/1.4931178

View online: <http://dx.doi.org/10.1063/1.4931178>

View Table of Contents: <http://scitation.aip.org/content/aip/journal/jcp/143/12?ver=pdfcov>

Published by the AIP Publishing

Articles you may be interested in

The interaction of organic adsorbate vibrations with substrate lattice waves in methyl-Si(111)-(1×1)
J. Chem. Phys. **141**, 024702 (2014); 10.1063/1.4886810

Structural and vibrational stability of M and Z phases of silicon and germanium from first principles
J. Appl. Phys. **113**, 193504 (2013); 10.1063/1.4804668

Vibrational dynamics of hydrogen on Ge surfaces
J. Chem. Phys. **130**, 134701 (2009); 10.1063/1.3102438

Density-functional theory study of vibrational relaxation of CO stretching excitation on Si(100)
J. Chem. Phys. **129**, 174702 (2008); 10.1063/1.2993254

Structure and binding energies of unsaturated hydrocarbons on Si(001) and Ge(001)
J. Chem. Phys. **124**, 024716 (2006); 10.1063/1.2151176

The logo for APL Photonics features the letters "AIP" in a large, bold, white font on the left, followed by a vertical yellow bar, and the journal title "APL Photonics" in a white serif font on the right. The background is a bright orange-red gradient with radiating yellow lines.

APL Photonics is pleased to announce
Benjamin Eggleton as its Editor-in-Chief



Vibrational dynamics and band structure of methyl-terminated Ge(111)

Zachary M. Hund,^{1,a)} Kevin J. Nihill,^{1,a)} Davide Campi,² Keith T. Wong,³ Nathan S. Lewis,³ M. Bernasconi,² G. Benedek,^{2,4} and S. J. Sibener^{1,b)}

¹The James Franck Institute and Department of Chemistry, The University of Chicago, 929 E. 57th Street, Chicago, Illinois 60637, USA

²Dipartimento di Scienza dei Materiali, Università di Milano-Bicocca, Via Cozzi 53, 20125 Milano, Italy

³Division of Chemistry and Chemical Engineering, Beckman Institute and Kavli Nanoscience Institute, California Institute of Technology, 210 Noyes Laboratory, 127-72, Pasadena, California 91125, USA

⁴Donostia International Physics Center (DIPC), Universidad del País Vasco (EHU), 20018 Donostia/San Sebastian, Spain

(Received 17 July 2015; accepted 31 August 2015; published online 25 September 2015)

A combined synthesis, experiment, and theory approach, using elastic and inelastic helium atom scattering along with *ab initio* density functional perturbation theory, has been used to investigate the vibrational dynamics and band structure of a recently synthesized organic-functionalized semiconductor interface. Specifically, the thermal properties and lattice dynamics of the underlying Ge(111) semiconductor crystal in the presence of a commensurate (1 × 1) methyl adlayer were defined for atomically flat methylated Ge(111) surfaces. The mean-square atomic displacements were evaluated by analysis of the thermal attenuation of the elastic He diffraction intensities using the Debye-Waller model, revealing an interface with hybrid characteristics. The methyl adlayer vibrational modes are coupled with the Ge(111) substrate, resulting in significantly softer in-plane motion relative to rigid motion in the surface normal. Inelastic helium time-of-flight measurements revealed the excitations of the Rayleigh wave across the surface Brillouin zone, and such measurements were in agreement with the dispersion curves that were produced using density functional perturbation theory. The dispersion relations for H-Ge(111) indicated that a deviation in energy and lineshape for the Rayleigh wave was present along the nearest-neighbor direction. The effects of mass loading, as determined by calculations for CD₃-Ge(111), as well as by force constants, were less significant than the hybridization between the Rayleigh wave and methyl adlayer librations. The presence of mutually similar hybridization effects for CH₃-Ge(111) and CH₃-Si(111) surfaces extends the understanding of the relationship between the vibrational dynamics and the band structure of various semiconductor surfaces that have been functionalized with organic overlayers. © 2015 AIP Publishing LLC. [http://dx.doi.org/10.1063/1.4931178]

I. INTRODUCTION

Crystalline semiconductors, including silicon and germanium, have played a crucial role in the electronics industry since the development of the transistor at Bell Laboratories in 1947. These materials also exhibit many properties that allow them to play a critical role in solar electricity generation.¹ Until recently, stable SiO₂ sites have allowed Si to become the semiconductor material of choice for field-effect devices, but now materials with larger dielectric constants are replacing SiO₂ (due to the relatively large Si/SiO₂ leakage current at the nanometer scale). Specifically, Ge has a 0.67 eV bandgap and is thus an attractive option for the collection of infrared radiation in multijunction solar cells.^{2,3} Additionally, the higher electron and hole mobilities (4 times larger than silicon) and lower processing temperatures of Ge relative to Si make Ge a desirable alternative for use in high-speed circuits as well as in metal-oxide-semiconductor field-effect transistors (MOSFETs).^{4,5}

However, a limiting factor that precludes facile fabrication of Ge-based devices is the rapid oxidation of the Ge surface that leads to water-soluble germanium oxides. Hence, to enable new opportunities for device applications, chemical control of the surface and interfacial properties is necessary to prevent oxidation and maintain the surface ordering of Ge crystals.

To minimize free energy, clean Ge(111) surfaces prepared under vacuum undergo reconstruction from a diamond cubic lattice structure to a c(2 × 8) surface configuration.⁶ However, chemical passivation of the Ge(111) surface via hydrogenation, bromination, or alkylation leads to a reconstruction of Ge(111) that returns to the native (1 × 1) unit cell. Hydrogen or bromine atoms can passivate all of the dangling bonds above the surface Ge atoms, providing enhanced stability against surface oxidation relative to clean Ge.^{7–9} The hydrogenated surface is sufficiently inert towards oxidation that H-Ge(111) can act as a reactive precursor for subsequent surface reactions, such as alkylation.¹⁰ For example, hydrogenated Ge(111) surfaces have been methylated using a two-step halogenation/alkylation process, creating well-ordered, air-stable surfaces with excellent electrical properties.^{11,12} Recently, highly ordered, atomically flat CH₃-Ge(111)-(1 × 1) surfaces

^{a)}Z. M. Hund and K. J. Nihill contributed equally to this work.

^{b)}Author to whom correspondence should be addressed. Electronic mail: s-sibener@uchicago.edu

have been prepared, resulting in improved chemical and electrical passivation.¹³

Several standard surface analytical techniques have revealed the chemical composition, surface structure, surface conductance, and methyl vibrational modes of methylated Ge(111) surfaces.^{11–14} X-ray photoelectron spectroscopy (XPS) indicates that the two-step halogenation/methylation process provides complete termination of the Ge surface sites by methyl groups.^{11–13} The vibrational modes of CH₃-Ge(111) have been investigated by use of transmission infrared spectroscopy (TIRS), high-resolution electron-energy loss spectroscopy (HREELS), and density functional perturbation theory (DFPT).^{12–14} Low-energy electron diffraction (LEED) indicates the formation of a hexagonal unit cell, whereas atomic force microscopy (AFM), scanning tunneling microscopy (STM), and helium atom diffraction all yield evidence for an atomic spacing of ~4.0 Å, confirming the (1 × 1) surface structure of CH₃-Ge(111).^{13,14} Additionally, methylated germanane (a single-layer crystal of germanium terminated with hydrogen) has recently been synthesized, and X-ray diffraction data indicate a hexagonal spacing with a lattice constant of $a = 3.96$ Å.¹⁵ Despite extensive structural characterization, the dynamics of CH₃-Ge(111) remain largely unexplored, whereas the dynamics of a surface analog, CH₃-Si(111), have been thoroughly studied both experimentally^{16–21} and theoretically.^{19,20,22}

We describe herein the comprehensive characterization of the dynamical properties of CH₃-Ge(111) to provide a foundation for understanding the thermal properties, energy accommodation at the interface, and vibrational band structure of such surfaces. Specifically, a combined scattering and theoretical study has been performed to characterize the vibrational dynamics and phonon band structure of this organic-functionalized Ge(111) interface. The vibrational features of methyl-terminated Ge(111) surfaces influence the thermal properties as well as the ability of the surface to accommodate energy. High-resolution helium atom scattering (HAS) and *ab initio* DFPT have been used herein to study the effects of methylation on the surface thermal motion and phonon band structure of the CH₃-Ge(111) surface. Extremely surface sensitive low-energy neutral helium diffraction measurements have been used to define the interfacial structure, gas-surface interaction potentials, and the temperature-dependent mean-square displacements (MSDs) both normal and parallel to the methylated surface. The phonon evolution of the Rayleigh wave across the surface Brillouin zone (SBZ) for two high-symmetry azimuthal alignments has been experimentally recorded because inelastic scattering of helium atoms, which is important in characterizing physical quantities such as the specific heat, thermal expansion coefficients, and electron-phonon interactions of a material,²³ is due to phonon (e.g., Rayleigh wave) excitations. These scattering measurements are found to be in agreement with the calculated phonon dispersions produced via density functional perturbation theory. DFPT was also used to generate the vibrational band structure for H-Ge(111) and CD₃-Ge(111), and these surfaces provided a comparison to CH₃-Ge(111) to elucidate the effects of mass loading, force constants, and adlayer vibrations. As seen previously for CH₃-Si(111) surfaces, the

hybridization with organic adlayer librations is the major influence that dictates the energy and lineshape of the surface phonon dispersions.

II. METHODS

The hydrogenation and subsequent alkylation of Ge(111) using a one-step alkylation from a H-Ge(111) precursor¹⁴ disproportionately etches the surface and yields a surface with a significant concentration of randomly distributed steps. The surfaces investigated herein were therefore instead prepared using a two-step halogenation-alkylation that produces atomically flat, methyl-terminated Ge(111) surfaces.¹³ Briefly, a thoroughly cleaned and rinsed Ge(111) wafer was hydrogenated by exposure to a flow of H₂ at 850 °C and atmospheric pressure. The sample was then cooled to below 100 °C. The resulting H-Ge(111) surface was brominated for 1 min at 50 °C in neat CCl₃Br that contained a small amount of benzoyl peroxide. The sample was rinsed with anhydrous tetrahydrofuran (THF) and then methylated in (CH₃)₂Mg/THF/1,4-dioxane for 5 min at 50 °C. For shipment from Pasadena, CA to Chicago, IL, the CH₃-Ge(111) surfaces were placed under high vacuum via turbo pumping the small stainless steel container prior to shipping. Upon receipt, the samples were immediately loaded into the ultra-high vacuum (UHV) sample chamber, with limited exposure to atmosphere in the interim.

Data were collected using an UHV helium atom scattering apparatus that provided high angular and energy resolution; this instrument and the range of its parameters have been thoroughly described elsewhere.²⁴ The crystal-to-ionizer distance was however shortened from 1.0234 m to 0.5705 m, which when added to a constant chopper-to-crystal distance of 0.4996 m, produced a total flight path of 1.0701 m (shortened from a total distance of 1.5230 m for the long mode). Inelastic helium time-of-flight experiments (described below) were performed with the detector in both configurations, providing greater angular resolution in the long mode, whereas greater intensity was produced in the short mode.

To collect the scattering data, helium gas was supersonically expanded into a series of differentially pumped chambers. The He was then scattered from a CH₃-Ge(111) crystal that had been mounted on a six-axis manipulator and temperature controlled with cryostatic cooling and a button heater, ionized by electron bombardment, and then filtered through a quadrupole mass spectrometer (QMS) before striking an electron multiplier. Prior to entering the sample chamber, the beam was mechanically modulated by a chopper wheel. For the elastic diffraction data that were used for Debye-Waller analysis, the beam was chopped with a 50% duty cycle for modulated detection. For collection of inelastic data, time-of-flight spectra were collected by chopping the beam with either a 50% duty cycle for cross-correlation analysis,²⁵ which used a pseudorandom 511 bit sequence of openings in the chopper wheel to increase signal-to-noise, or by use of a 1% duty cycle for a single-slit pattern. For single-shot time-of-flight runs, composite spectra were often produced to increase the signal-to-noise by adding multiple spectra taken under identical incidence conditions. The temperature of the sample

was flashed to 450 K between runs to eliminate unwanted surface adsorbates.

The dynamical properties of the H-Ge(111), CH₃-Ge(111), and CD₃-Ge(111) surfaces were calculated using density functional perturbation theory, as implemented in the QUANTUM-ESPRESSO package²⁶ using a norm-conserving pseudopotential for Ge, ultrasoft pseudopotentials²⁷ for C and H, and the Perdew-Burke-Ernzerhof (PBE) approximation²⁸ for the exchange-correlation energy functional. The electronic wavefunctions were expanded in plane waves up to a 28 Ry energy cutoff and a 280 Ry charge-density cutoff. The surfaces were modeled with a slab geometry and periodic boundary conditions (PBCs), and the slabs were composed of 18 germanium atom layers with hydrogen or methyl groups adsorbed on both sides, which were separated by a 12 Å-wide vacuum gap.¹⁴ The SBZ was sampled over a Monkhorst-Pack grid of 6 × 6 × 1 k-points.²⁹ The atomic positions were relaxed until the forces were below a 5 × 10⁻⁵ a.u. threshold. The dynamical matrix was calculated on a 6 × 6 × 1 q-point mesh for the SBZ. The Fourier transform of the dynamical matrices on a discrete uniform mesh in the SBZ provided the real-space interatomic force constants that allowed calculation of the dispersion relations.

III. RESULTS AND DISCUSSION

A. Vibrational dynamics

He diffraction of CH₃-Ge(111) surfaces has previously indicated the presence of a hexagonally packed methyl adlayer with a (1 × 1) methyl termination of the Ge(111) lattice.¹⁴ Figure 1 shows diffraction spectra that include first-, second-, and zeroth-order diffraction peaks for the high-symmetry ⟨1̄2̄1⟩ and ⟨01̄1⟩ azimuthal alignments. These alignments and their corresponding diffraction peaks were used for the experiments reported on herein.

The diffraction patterns show the helium reflectivity as a function of the parallel momentum transfer,

$$\Delta \vec{K} = \vec{k}_i (\sin(\theta_f) - \sin(\theta_i)) \quad (1)$$

where \vec{k}_i is the incident helium beam wavevector, and θ_i and θ_f are the initial and final scattering angles, respectively. The ΔK spacing of 1.82 Å⁻¹ observed between the diffraction peaks for the ⟨1̄2̄1⟩ alignment (Figure 1) is consistent with a 4.00 Å real-space lattice constant, confirming the presence of a hexagonally packed (1 × 1) methyl adlayer. Figure 1(c) shows a proposed top-view model of the CH₃-Ge(111) surface. The sharp and large diffraction peak intensities, along with a minimal diffuse background, suggest the formation of a low-defect surface with long-range ordering. These large intensities are required to extract information on the surface dynamics via thermal attenuation measurements.

The thermal attenuation of the diffraction peaks provides information on the vibrational dynamics of the surface, because the diffraction peak intensity decays with increasing sample temperature as the vibrational amplitude of the surface oscillators increases, resulting in inelastic scattering of the impinging helium atoms.³⁰ The surface temperature, T_s , of CH₃-Ge(111) was varied ($T_s = 200$ –500 K) at five different

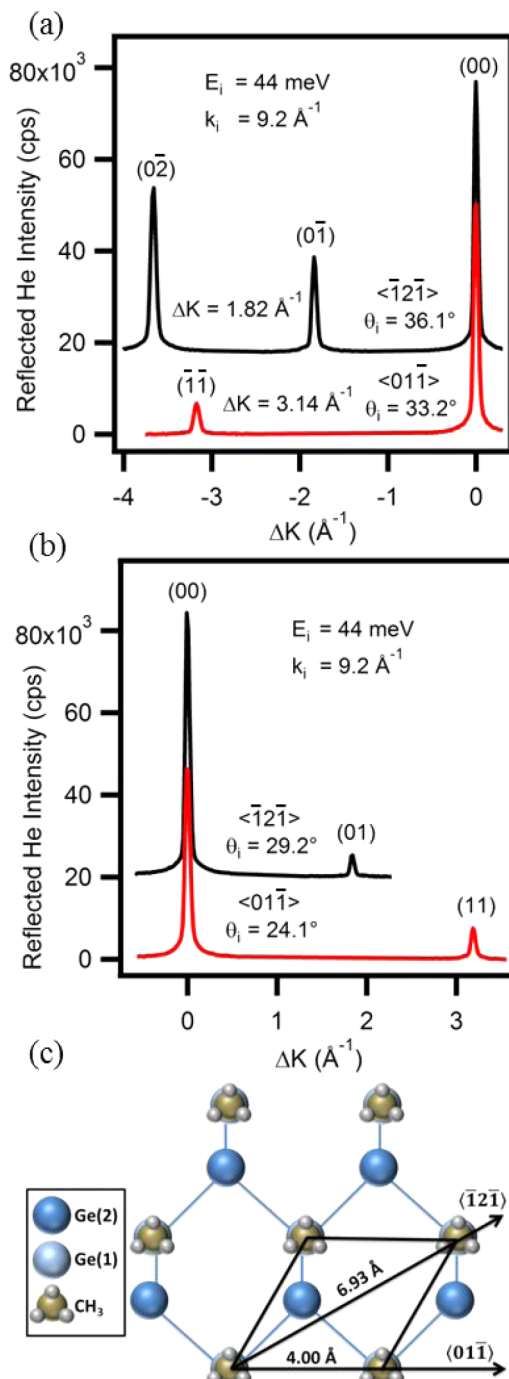


FIG. 1. (a) He diffraction spectra showing the back-scattered (negative) diffraction peaks along both primary azimuthal alignments with corresponding peak spacings; (b) diffraction spectra showing the forward-scattered (positive) diffraction peaks along both azimuthal alignments; (c) top-view model of the CH₃-Ge(111) surface with real lattice spacings.

incident beam angles between diffraction scans to calculate the Debye-Waller factor, $W(T_s)$. The observed diffraction peak intensity, I , is exponentially dependent on the Debye-Waller factor, such that

$$I = I_0 e^{-2W(T_s)}, \quad (2)$$

where I_0 is the peak intensity at a theoretical surface temperature of 0 K. The Debye-Waller factor is comprised of four components: the normal and parallel momentum transfers during the scattering process, Δk_z and ΔK , respectively, and

their associated MSDs of the crystal atoms, $\langle u_z^2 \rangle$ and $\langle u_{\parallel}^2 \rangle$,

$$2W(T_s) = \Delta k_z^2 \langle u_z^2 \rangle + \Delta K^2 \langle u_{\parallel}^2 \rangle, \quad (3)$$

where

$$\Delta \vec{k}_z = \vec{k}_i \left[\left(\cos^2 \theta_i + \frac{D}{E_i} \right)^{1/2} + \left(\cos^2 \theta_f + \frac{D}{E_i} \right)^{1/2} \right]. \quad (4)$$

Here, the D/E_i term accounts for acceleration of a He atom with energy E_i as the atom enters the attractive portion of the gas-surface potential well having a depth D .³¹ When only the thermal attenuation of the specular ($\theta_i = \theta_f$) peak (Figure 2(a)) is observed, the parallel momentum transfer to the surface is assumed to be zero, allowing simplification of Equations (3) and (4) to yield

$$2W(T_s) = \Delta k_z^2 \langle u_z^2 \rangle, \quad (5)$$

$$\Delta \vec{k}_z = 2 \vec{k}_i \left[\left(\cos^2 \theta_i + \frac{D}{E_i} \right)^{1/2} \right]. \quad (6)$$

According to Equation (2), plotting the natural log of $I(T_s)/I_0$ as a function of the surface temperature should result in a linear relationship. Figure 2(b) shows linear decays of the total peak area with respect to increases in the surface temperature, confirming that the Debye-Waller model held for the experimental range of surface temperatures in this system. Each diffraction pattern was recorded with a 44 meV helium beam and was repeated three separate times at five different incident angles ($\theta_i = 22.1^\circ, 26.1^\circ, 29.1^\circ, 32.6^\circ$, and 36.1°). Taking the derivative of Equation (5) with respect to the surface temperature reveals the surface temperature-dependence of the Debye-Waller factor,

$$\sigma = -\frac{d(2W)}{dT_s} = -\left[\Delta k_z^2 \frac{d\langle u_z^2 \rangle}{dT_s} \right]. \quad (7)$$

The expression for the exchange of perpendicular momentum (Equation (6)) can then be inserted to produce the desired relationship

$$\sigma = 4k_i^2 \frac{d\langle u_z^2 \rangle}{dT_s} \left[\cos^2 \theta_i + \frac{D}{E_i} \right], \quad (8)$$

such that a linear fit of the Debye-Waller decay, σ , versus $\cos^2 \theta_i$ can be used to determine the temperature dependent

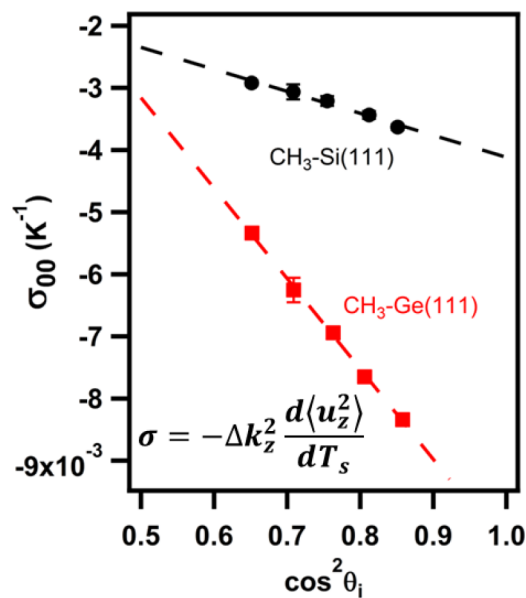


FIG. 3. Decay rate of specular intensity as a function of the squared cosine of the incidence angle, showing a greater dependence on angle for CH₃-Ge(111) as compared with CH₃-Si(111), indicating a softer interface. Error bars represent standard deviations from independent measurements repeated three times for each point.

mean-square displacement and potential well depth from the slope and y-intercept, respectively, of the data.

Figure 3 shows the angular dependence of the Debye-Waller factor for the CH₃-Ge(111) surface.¹⁷ A linear fit to the specular data yielded a slope of -0.0145 K^{-1} and an intercept of 0.0041. Given $k_i = 9.2 \text{ \AA}^{-1}$, $d\langle u_z^2 \rangle/dT_s$ is $(4.3 \pm 0.2) \times 10^{-5} \text{ \AA}^2 \text{ K}^{-1}$ for the CH₃-Ge(111)-(1 \times 1) surface. For comparison, a previous He diffraction study identified a perpendicular MSD of $\sim 1.5 \times 10^{-5} \text{ \AA}^2 \text{ K}^{-1}$ (based on extrapolation of their diffraction data) for Ge(111)-c(2 \times 8).³² The perpendicular MSD of the CH₃-Ge(111)-(1 \times 1) surface shows a significant deviation from that of Ge(111)-c(2 \times 8), which is consistent with the decreased effective surface mass (72 amu for Ge, now 15 amu for CH₃) and an increase in the surface Debye temperature, as discussed in detail below. In the harmonic limit of the Debye-Waller model, the MSD is inversely proportional to the effective surface mass as well as to the square of the Debye temperature. The mass reduction

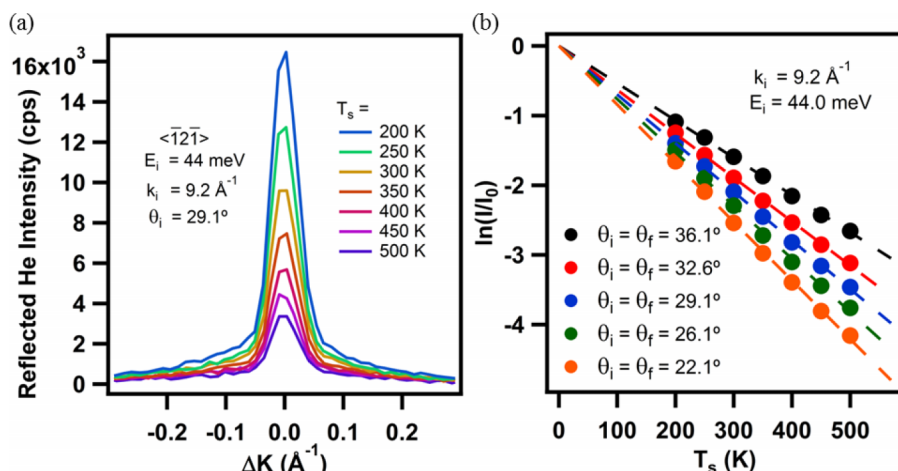


FIG. 2. (a) Decay of the specular ($\theta_i = \theta_f$) diffraction peak as a function of CH₃-Ge(111) surface temperature, plotted vs. parallel component of momentum exchange; (b) natural log of specular decay with respect to total intensity for five different incidence angles; data exhibit a linear decrease with increasing sample temperature and a greater rate of signal decay for a more normal incidence angle.

by a factor of five thus overwhelms a less than doubled surface Debye temperature, accounting for an increase in the perpendicular MSD. Additionally, Ohkuma and Nakamura³³ have shown that surface reconstruction of diamond-structure crystals can suppress the perpendicular MSD, causing an even larger deviation between the two values. As shown by Figure 3, the perpendicular MSD for CH₃-Ge(111) is approximately four times larger than that of $(1.0 \pm 0.1) \times 10^{-5} \text{ \AA}^2 \text{ K}^{-1}$ for CH₃-Si(111).¹⁷ This deviation arises from the lesser effective mass reduction (28 amu for Si, now 15 amu for CH₃), with a similarly large increase in its Debye temperature. Hence, methyl-termination of Si(111) instead results in a decrease of the perpendicular MSD relative to the bulk value for Si(111) (7×7). Although functionalization of both surfaces causes a decrease in their effective masses to different degrees, the still-present perpendicular stiffness of both methyl-terminated surfaces is associated with the rigidity of their directional, sp³-hybrid Si/Ge-C covalent bonds.

Due to the large slope observed for CH₃-Ge(111) (Figure 3), the y-intercept extracted from the Debye-Waller model does not provide a realistic value for the He potential well depth. This arises from the inability of such Debye-Waller measurements to properly account for the low-temperature librational dynamics of the system. A well depth of ~ 7.5 meV has been measured for similarly functionalized CH₃-Si(111)¹⁷ and H-Si(111) surfaces.³⁴ The He scattering potential is a function of the surface electron density,³⁵ which we expect to be similar for CH₃-Ge, so a well depth of 7.5 meV has been assumed herein. By inserting the parallel momentum component from Equation (3) into Equation (7), the parallel MSD can be calculated and separated from the perpendicular MSD component. Figure 4 shows representative thermal attenuation diffraction spectra for two non-specular diffraction peaks. The temperature-dependent decay in the areas of these peaks was compared with similar spectra that measured other first- and second-order peaks at a range of surface temperatures and provided an average parallel MSD of $(2.2 \pm 1.6) \times 10^{-3} \text{ \AA}^2 \text{ K}^{-1}$. The parallel MSD was found to be

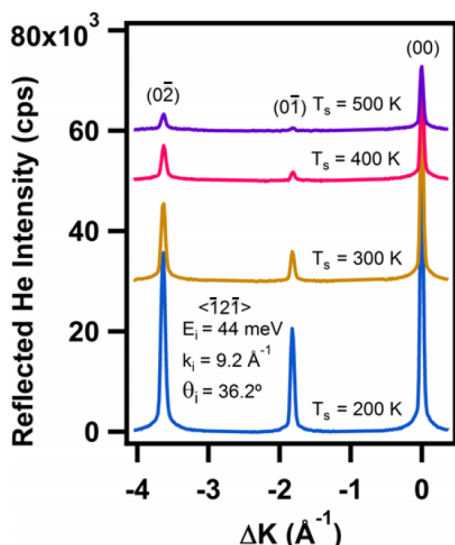


FIG. 4. Decay of the specular and first- and second-order diffraction peaks for the same incidence energy.

nearly two orders of magnitude larger than the perpendicular MSD of $(4.3 \pm 0.2) \times 10^{-5} \text{ \AA}^2 \text{ K}^{-1}$ measured herein for CH₃-Ge(111). Recent theoretical studies on methyl-terminated semiconductor surfaces have proposed couplings between methyl bending vibrational modes and the underlying lattice waves, thereby significantly increasing the surface thermal motion in the parallel direction, as observed here.^{19,22} These larger parallel MSDs suggest that the surface shares librational characteristics with not only the previously studied methyl silicon system but also with other organic overlayers on metals.³⁶

For a classical harmonic oscillator, the Debye-Waller model can also be expressed as

$$W(T_s) = \frac{12m [E_i \cos^2 \theta_i + D] T_s}{M_{\text{eff}} k_B \Theta_D^2}, \quad (9)$$

where m is the mass of the incident helium atom, M_{eff} is the effective surface mass, k_B is Boltzmann's constant, and Θ_D is the surface Debye temperature. The Debye temperature of the CH₃-Ge(111) surface is calculated to be 689 ± 20 K (479 cm^{-1}), given that the effective mass that a helium atom collides with decreases from 72 amu for Ge(111) to 15 amu for CH₃-Ge(111), and the estimated potential well depth is 7.5 meV. This value is significantly larger than the value of ~ 360 – 374 K that has been measured for the Debye temperature of bulk Ge(111).^{37,38} Additionally, RHEED measurements give an effective surface Debye temperature of 96 K for clean c(2×8)-Ge(111) surfaces, which was proposed to be due to the weakening of the harmonic force constant of the interlayer potential.³⁹ Therefore, instead of producing a softer Ge(111) surface, methyl termination imposes a greater rigidity, as indicated by a nearly doubled Debye temperature for the surface. This rigidity can be explained by the coupling of impinging helium atoms to the vibrational modes of the terminated methyl groups. The calculated surface Debye temperature (479 ± 14 cm⁻¹) is in accord with the Ge-C stretching mode frequency for CH₃-Ge(111) measured with HREELS¹³ (568 cm⁻¹) and DFT¹⁴ (530 cm⁻¹), as well as in accord with IR data for methylgermane⁴⁰ (601.6 cm⁻¹). By terminating the Ge(111) lattice with methyl groups, the collisional dynamics have changed such that helium atoms strongly interact with localized molecular modes rather than just interacting with low-energy phonons that originate from the lattice.

B. Phonon band structure

The vibrational motion and band structure of surface groups can be additionally characterized by the use of inelastic helium atom scattering, which involves the transfer of both energy and momentum between an impinging He atom and the surface. The extreme sensitivity of HAS to sagittal displacement (shear vertical motion of surface atoms) allows for strongly resolved measurements of the Rayleigh wave, which is the lowest-energy surface acoustic mode that vibrates in the sagittal plane. The relatively short wavelength and small penetration of the Rayleigh wave make it especially sensitive to interatomic forces at the surface; hence, measurement of the Rayleigh wave provides insight into the interaction of the surface methyl groups with the underlying germanium

lattice. Hence, inelastic helium atom scattering was used to map out the surface phonon dispersion curves for CH₃-Ge(111) along both the $\langle\bar{1}\bar{2}\bar{1}\rangle$, Γ -M, and $\langle 01\bar{1}\rangle$, Γ -K, primary azimuthal directions across the SBZ.

The inelastic scattering data were extracted from a series of time-of-flight spectra taken over a large range of kinematic conditions. Figure 5 shows representative composite inelastic single-shot time-of-flight spectra that were recorded at seven different final scattering angles for the same beam energy and sample temperature. Each spectrum exhibited a large diffuse elastic peak, as well as two sharp inelastic peaks on either side, indicating single-phonon interactions with the Rayleigh wave. Each of these peaks was located atop a broad inelastic background formed by multiple-phonon excitations, which is consistent with expectations based on the soft nature of the surface, as indicated by the Debye-Waller experiments detailed above.

The time-of-flight spectra readily provide the energy and parallel momentum that is exchanged with the surface in an inelastic scattering process. The flight times of elastic and single-phonon creation and annihilation peak maxima were determined by least-squares fitting the data with multiple Gaussian peaks, with the multiphonon background subtracted, to leave a fairly flat residual. The fitted flight times were then referenced to the length of the flight path from the crystal to the detector to calculate the associated energy exchanges with the surface. The conservations of energy and surface parallel momentum for single-phonon interactions,

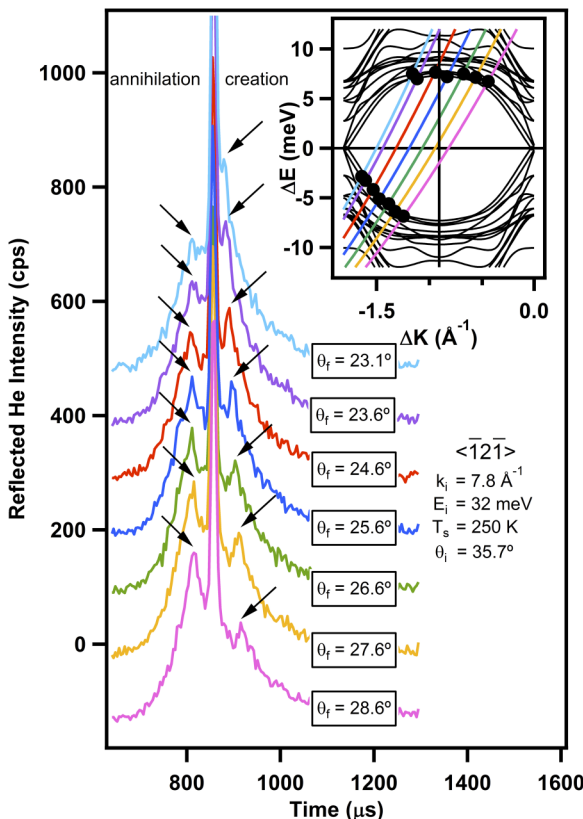


FIG. 5. Inelastic time-of-flight spectra of several final scattering angles (θ_f), offset vertically for clarity; arrows indicate single-phonon annihilation and creation peaks, corresponding to the black dots in the dispersion curve (inset), which themselves fall on color-coded scan curves for each spectrum.

$$\vec{k}_f^2 = \vec{k}_i^2 + \frac{2m}{\hbar^2} \hbar \omega (\vec{Q}), \quad (10)$$

$$\vec{k}_f = \vec{K}_i + \vec{G}_{mn} + \vec{Q}, \quad (11)$$

where $\hbar \omega (\vec{Q})$ is the energy of a phonon with wavevector \vec{Q} and frequency ω ($\omega < 0$ indicates creation of a phonon and $\omega > 0$ an annihilation), were then combined to yield an expression that describes the functional form of a scan curve,

$$\frac{\hbar \omega (Q)}{E_i} = \frac{\sin^2 \theta_i}{\sin^2 \theta_f} \left(1 + \frac{\Delta K}{K_i} \right) - 1. \quad (12)$$

Scan curves calculate the allowed exchange of surface parallel momentum as a function of the known phonon energy and kinematic parameters and delineate the possible single-phonon events that may be observed experimentally. Such data are presented in the inset of Figure 5 as colored bands that correspond to the conditions of their respective time-of-flight spectra.

The experimental data in the inset of Figure 5 agree very well with the dispersion curves provided by the DFPT calculations and show a clear dispersion of the Rayleigh wave across the $\langle\bar{1}\bar{2}\bar{1}\rangle$ region of the SBZ. The increasing temporal distance between the elastic and inelastic creation peaks in the time-of-flight spectra results from a greater exchange of momentum and energy with the surface, causing the phonon data to disperse away from the zone center (Γ -point) in the dispersion curve. Moreover, the increase in surface parallel momentum and energy exchange causes the intensity of the Rayleigh wave peak to decrease considerably, as has been demonstrated elsewhere.⁴¹ Conversely, the annihilation time-of-flight peaks initially moved away from the elastic peak, but then dispersed back towards the elastic peak (beginning at $\theta_i = 24.6^\circ$) as the phonons crossed over the M-point ($|\Delta K| = 0.907 \text{ \AA}^{-1}$) in the dispersion curve. These inelastic transitions involving *umklapp* phonons are expected for surfaces with high corrugation, as reported elsewhere.⁴² These *umklapp* phonons are folded into the irreducible surface Brillouin zone along with the entire inelastic data set, as shown in Figure 6.

Density functional perturbation theory was used to calculate the vibrational band structure for CH₃-Ge(111). The absolute energies of all experimental single-phonon processes are displayed on the reduced dispersion curves in Figure 6, which have been color-coded to represent the total degree of sagittal polarization at the surface. A large degree of the sagittal vibrational motion clearly arises from the Rayleigh wave, the lowest-energy dispersion curve. Within experimental error (less than 0.5 meV), the large amount of experimental inelastic data agrees with the theoretical dispersion curves, clearly mapping out the Rayleigh wave across the SBZ, along with a few higher-energy modes. The inability to completely map out the Rayleigh wave in the $\overline{\Gamma K}$ and \overline{KM} regions is explained by a lower degree of sagittal displacement. Additionally, the low-energy Rayleigh wave is difficult to experimentally resolve from the significant bulk band excitations and multiphonon contributions introduced by the aforementioned corrugation and relative softness of the surface.⁴³ Likewise, single phonons occurring at higher-energy areas of strong sagittal displacement (such as at the K-point, ~12 and 14 meV) require higher beam energies to

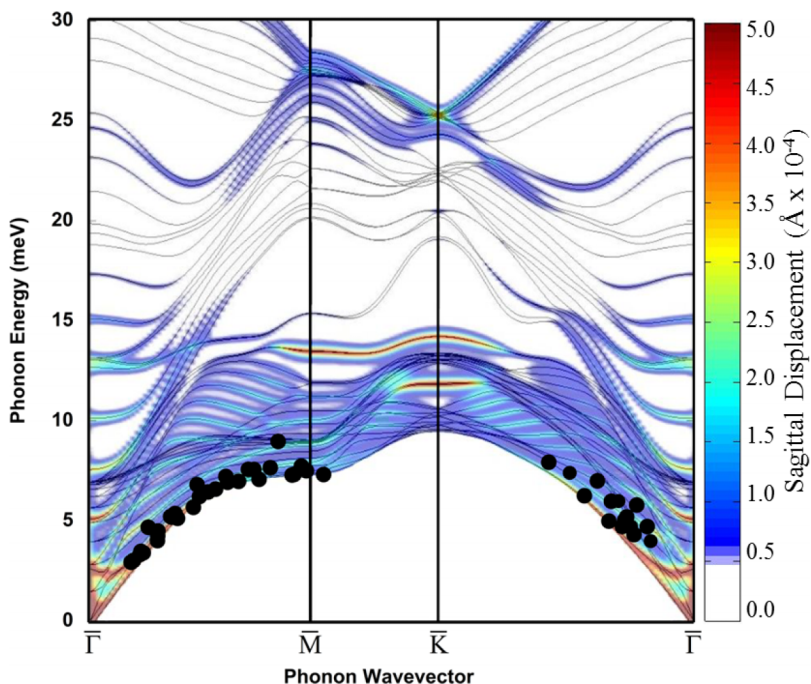


FIG. 6. Dispersion curves (lines) of $\text{CH}_3\text{-Ge}(111)$ as determined by DFPT calculations, overlaid with HAS single phonon data collected in the same manner as in Fig. 3; total sagittal displacement of the CH_3 group is indicated by color bar.

excite, but are washed out by the simultaneous excitation of multiple lower-energy modes, as higher beam energies increase the Weare parameter beyond the threshold of single-phonon domination.⁴⁴

The Debye-Waller measurements reported above indicate a considerably softer surface for $\text{CH}_3\text{-Ge}(111)$ relative to $\text{CH}_3\text{-Si}(111)$, an analog hybrid organic-semiconductor interface. The relative softness of $\text{CH}_3\text{-Ge}(111)$ is reflected in the overall lower energy of the Rayleigh wave, in that the calculated energies at the \bar{M} - and \bar{K} -point are 7.3 and 9.6 meV, respectively, for $\text{CH}_3\text{-Ge}(111)$, whereas these values are approximately twice as large for $\text{CH}_3\text{-Si}(111)$, at 13.3 and 17.9 meV.¹⁹ As detailed elsewhere,⁴³ the Rayleigh wave can be reproduced fairly accurately by a force constant model for a single atomic layer with nearest- and next-nearest-neighbor interactions. This disparity in the Rayleigh wave energies should therefore be reflected in the force constants of the two surfaces. Wei and Chou⁴⁵ created an 8×8 supercell and used the Hellmann-Feynman theorem to calculate the transverse force constants for surface atoms of bare $\text{Ge}(111)$ (-1.937 dyn/cm) and $\text{Si}(111)$ (-2.193 dyn/cm), which strengthens this hypothesis of softening. Additionally, Han *et al.*⁴⁶ noted that the largest phonon energy in Ge (38 meV) is only about 60% of that in Si (64 meV), which matches well with the relative Rayleigh wave zone-edge energies of these two methyl-terminated interfaces.

Phonon dispersions for clean $\text{Ge}(111)$ have been measured experimentally^{6,47,48} and theoretically.⁴⁵ Clean $\text{Ge}(111)$ reconstructs rapidly, which causes distortions of the dispersion curves;⁴⁹ however, at high temperatures, $\text{Ge}(111)$ recovers the (1×1) structure such that the Rayleigh wave dispersion curves measured by HAS at 1000 K⁴⁸ can be directly compared with the present data for $\text{CH}_3\text{-Ge}(111)$ at low temperatures. There is a surprising agreement between the Rayleigh wave data in both cases, indicating that the anharmonic softening expected for the clean $\text{Ge}(111)$ at high temperature is comparable to

that due to the mass loading effect of the methyl adlayer at low temperatures. To better understand the relationship between organic functionalization and the vibrational band structure of germanium, the results for $\text{CH}_3\text{-Ge}(111)$ have been compared with $\text{H-Ge}(111)-(1 \times 1)$. In the case of $\text{H-Ge}(111)$, surface atoms preserve the ideal tetrahedral configuration of the unreconstructed (1×1) surface, which ought to exhibit dynamics similar to those of the clean (1×1) semiconductor surface,⁵⁰ such that adlayer interactions do not significantly affect the vibrational characteristics of the semiconductor lattice. In the absence of measurements of the surface phonon relations for hydrogen-terminated germanium, the vibrational band structure for $\text{H-Ge}(111)-(1 \times 1)$ has been constructed in this work by the use of DFPT. Figure 7 compares the low-energy vibrational band structure of $\text{H-Ge}(111)$ and $\text{CH}_3\text{-Ge}(111)$, with the color scale indicating the relative sagittal displacement of their respective 1st layer Ge atoms.

Although the Rayleigh wave frequency is nearly identical for both terminated surfaces at the \bar{M} point, methylation of the $\text{Ge}(111)$ surface produces a noticeable increase in the Rayleigh wave energy along the $\bar{\Gamma}\bar{K}$ azimuth near the zone edge (\bar{K} point). This deviation can be attributed to three sources: changes in the local force constants, mass-loading effects, and/or hybridization between lattice and adlayer vibrations. Methyl termination results in the addition of only 0.04 electrons to the $\text{Ge}-\text{Ge}$ bonds in the first two layers with respect to clean $\text{Ge}(111)-(1 \times 1)$. Comparison of $\text{H-Ge}(111)$ and $\text{CH}_3\text{-Ge}(111)$ surfaces displays similar Ge lattice charge densities, as seen with DFPT; as a result, the force constants for $\text{CH}_3\text{-Ge}(111)$ are only 2.5% and 2.2% weaker in-plane and out-of-plane, respectively, than $\text{H-Ge}(111)$. Modifications of the local force constants due to methyl termination are therefore not primarily responsible for the increase in phonon energy observed for $\text{CH}_3\text{-Ge}(111)$. Additionally, the DFPT-calculated displacement fields did not display a linear sagittal polarization at the \bar{M} point, which would be expected for a

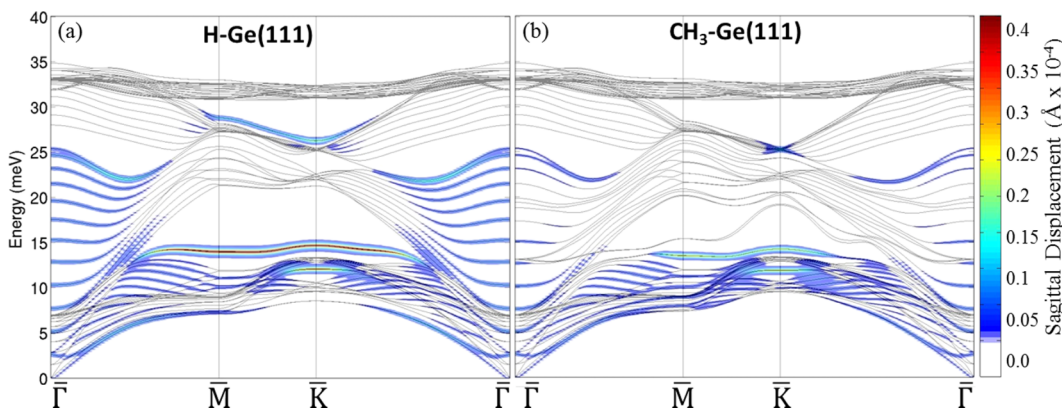


FIG. 7. Dispersion curves of (a) H-Ge(111) and (b) CH₃-Ge(111) as determined by DFPT calculations; relative sagittal displacements of 1st layer Ge atoms indicated by color bar.

Rayleigh wave associated with an ideal fcc surface.²³ Our previous work on methyl-terminated Si(111) showed that the deviation in the shape and energy of the Rayleigh wave for CH₃-Si(111) from H-Si(111) was a result of hybridization of the Si(111) lattice waves with methyl adlayer rocking librations.¹⁹ This mechanism can hence be formally extended to the Ge(111) system, where the rocking libration of the terminated methyl group (characterized by a slight distortion of the internal C-H bonds and the bending of the C-Ge bond with an energy of 13.1 meV at the $\bar{\Gamma}$ point) has coupled with the lattice waves near the zone edge to induce an observable deviation of the Rayleigh wave along the $\Gamma\bar{K}$ alignment. The hybridization is slightly weaker for Ge(111) than Si(111), because the hybridization in CH₃-Si(111) caused an increase of nearly 2 meV at the \bar{K} point for the Rayleigh wave, whereas the hybridization for CH₃-Ge(111) only resulted in an increase of about 1.5 meV relative to H-Ge(111). This weaker hybridization is attributed to the lower energy of the CH₃-Ge(111) Rayleigh wave, causing an increased energy difference between the methyl vibrational modes and the Rayleigh wave.

To account for mass-loading contributions of the terminal methyl groups to the underlying lattice wave dispersions, DFPT was used to produce the vibrational band structure

for CD₃-Ge(111), a simple isotopic analog of CH₃-Ge(111). Experimental comparisons with the theory data for CD₃-Ge(111) have not yet been performed due to difficulties in synthesizing high-quality crystals with near-complete CD₃ termination, thereby prohibiting resolved inelastic helium scattering measurements. Figure 8 compares the vibrational band structure for CH₃-Ge(111) and CD₃-Ge(111), with the color scale representing the relative sagittal displacement of the C atoms in each system. The Rayleigh wave frequency should scale as $C^{1/2}M_{\text{eff}}^{-1/2}$, where C is the interatomic force constant and M_{eff} is the effective mass. For the Rayleigh wave, the effective mass can be taken as the mass of a single germanium atom with a single methyl group. This approach is taken from the comparison between data for CD₃- and CH₃-Si(111) surfaces, where the increased mass (43 amu for CH₃-Ge and 46 amu for CD₃-Si) resulted in an energy decrease of 17.9–17.3 meV for CD₃-Si(111). Applying the same approach here, the smaller deviation in mass (87 amu for CH₃-Ge and 90 amu for CD₃-Ge) becomes negligible, suggesting a decrease in the Rayleigh wave frequency of only ~ 0.16 meV. Figure 8 consistently provides evidence for this rather small decrease in the Rayleigh wave energy, demonstrating that mass-loading effects play a minimal role in determining the energies of the Rayleigh wave dispersion

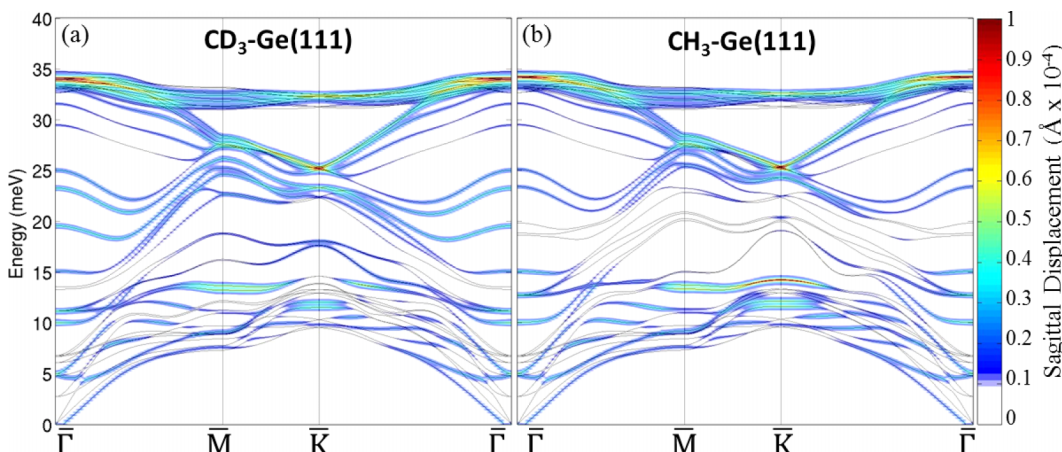


FIG. 8. Dispersion curves of (a) CD₃-Ge(111) and (b) CH₃-Ge(111) as determined by DFPT calculations; relative sagittal displacements of C atoms indicated by color bar.

for CH₃-Ge(111). One notable difference in the band structure for CH₃-Si(111) vs CD₃-Si(111) is the presence of a mode crossing between the Rayleigh wave and a hindered methyl rotation. The crossing is absent for CD₃-Ge(111) due to the much lower energy of its Rayleigh wave compared to CD₃-Si(111), while the hindered rotational mode is only slightly decreased (13.8 meV for CD₃-Ge(111) and 20.8 meV for CD₃-Si(111)) due to the larger Ge lattice constant and therefore reduced interaction between neighboring methyl groups. Overall, analysis of the H-Ge(111), CH₃-Ge(111), and CD₃-Ge(111) band structures indicates that hybridization of modes is the primary influence in determining the Rayleigh wave dispersion, with mass loading and force changes contributing negligibly. This phenomenon has now been extended from CH₃-Si(111) to CH₃-Ge(111) and is likely present for other organically functionalized group IV semiconductors.¹⁰

IV. CONCLUSIONS

This combined experimental and theoretical effort has revealed the vibrational dynamics and band structure of the atomically flat CH₃-Ge(111) interface. The attenuated intensities of helium atom diffraction peaks at a variety of incidence angles were exponentially dependent on increasing surface temperature, allowing for the application of the Debye-Waller model to this hybrid organic-semiconductor interface. This approach allowed for a precise estimation of the surface Debye temperature as well as an estimation of the temperature-dependent atomic displacements of the surface methyl groups in both the surface-normal and -parallel directions, which indicated a transition in the regime of surface motion enforced by the methyl adlayer. Inelastic helium scattering measurements were complemented with high-level density functional perturbation theory calculations, showing agreement in the mapping of the phonon dispersion of the Rayleigh wave across the surface Brillouin zone. The minimal effects of mass loading on the lattice waves were resolved by producing the vibrational band structure for an isotopically substituted surface, CD₃-Ge(111). Comparing the surface phonon dispersions of CH₃-Ge(111) and H-Ge(111) aided in the identification of hybridization of methyl adlayer librations with the Rayleigh wave as the dominant factor in shaping the Rayleigh wave dispersion, which agrees with similar effects observed for CH₃-Si(111). The results collectively strengthen the understanding of the relationship between the nature of the organic functionalization and the vibrational dynamics and phonon band structure of Ge(111) and can be applied to other group IV semiconductors as well.

ACKNOWLEDGMENTS

S.J.S. acknowledges support from the Air Force Office of Scientific Research Grant Nos. FA9550-10-1-0219 and FA9550-15-1-0428, and the Material Research Science and Engineering Center at the University of Chicago, Grant No. NSF-DMR-14-20709. N.S.L. acknowledges support from the National Science Foundation (Grant No. CHE-1214152), and research was in part carried out at the Molecular Materials

Research Center of the Beckman Institute of the California Institute of Technology.

- ¹M. Riordan, L. Hoddeson, and C. Herring, *Rev. Mod. Phys.* **71**, S336 (1999).
- ²W. Guter, J. Schöne, S. P. Philippss, M. Steiner, G. Siefer, A. Wekkeli, E. Welser, E. Oliva, A. W. Bett, and F. Dimroth, *Appl. Phys. Lett.* **94**, 223504 (2009).
- ³R. R. King, D. C. Law, K. M. Edmondson, C. M. Fetzer, G. S. Kinsey, H. Yoon, R. A. Sherif, and N. H. Karam, *Appl. Phys. Lett.* **90**, 183516 (2007).
- ⁴A. Delabie, F. Bellenger, M. Houssa, T. Conard, S. Van Elshocht, M. Caymax, M. Heyns, and M. Meuris, *Appl. Phys. Lett.* **91**, 082904 (2007).
- ⁵K. Kita, S. Suzuki, H. Nomura, T. Takahashi, T. Nishimura, and A. Toriumi, *Jpn. J. Appl. Phys. Part 1* **47**, 2349 (2008).
- ⁶D. Farías, G. Lange, K. H. Rieder, and J. P. Toennies, *Phys. Rev. B* **55**, 7023 (1997).
- ⁷P. W. Loscutoff and S. F. Bent, *Annu. Rev. Phys. Chem.* **57**, 467 (2006).
- ⁸R. D. Bringans and H. Höchst, *Appl. Surf. Sci.* **11-12**, 368 (1982).
- ⁹S. Sun, Y. Sun, Z. Liu, D.-I. Lee, and P. Pianetta, *Appl. Phys. Lett.* **89**, 231925 (2006).
- ¹⁰G. W. Cullen, J. A. Amick, and D. Gerlich, *J. Electrochem. Soc.* **109**, 124 (1962).
- ¹¹D. Knapp, B. S. Brunschwig, and N. S. Lewis, *J. Phys. Chem. C* **114**, 12300 (2010).
- ¹²D. Knapp, B. Brunschwig, and N. S. Lewis, *J. Phys. Chem. C* **115**, 16389 (2011).
- ¹³K. T. Wong, Y.-G. Kim, M. P. Soriaga, B. S. Brunschwig, and N. S. Lewis, *J. Am. Chem. Soc.* **137**, 9006 (2015).
- ¹⁴Z. M. Hund, K. J. Nihill, D. Campi, K. T. Wong, N. S. Lewis, M. Bernasconi, G. Benedek, and S. J. Sibener, *J. Phys. Chem. C* **119**, 18458 (2015).
- ¹⁵S. Jiang, S. Butler, E. Bianco, O. D. Restrepo, W. Windl, and J. E. Goldberger, *Nat. Commun.* **5**, 1 (2014).
- ¹⁶L. J. Webb, S. Rivillon, D. J. Michalak, Y. J. Chabal, and N. S. Lewis, *J. Phys. Chem. B* **110**, 7349 (2006).
- ¹⁷J. S. Becker, R. D. Brown, E. Johansson, N. S. Lewis, and S. J. Sibener, *J. Chem. Phys.* **133**, 104705 (2010).
- ¹⁸R. D. Brown, Q. Tong, J. S. Becker, M. A. Freedman, N. A. Yufa, and S. J. Sibener, *Faraday Discuss.* **157**, 307 (2012).
- ¹⁹R. D. Brown, Z. M. Hund, D. Campi, L. E. O'Leary, N. S. Lewis, M. Bernasconi, G. Benedek, and S. J. Sibener, *Phys. Rev. Lett.* **110**, 156102 (2013).
- ²⁰R. D. Brown, Z. M. Hund, D. Campi, L. E. O'Leary, N. S. Lewis, M. Bernasconi, G. Benedek, and S. J. Sibener, *J. Chem. Phys.* **141**, 024702 (2014).
- ²¹S. Malyk, F. Y. Shalhout, L. E. O'Leary, N. S. Lewis, and A. V. Benderskii, *J. Phys. Chem. C* **117**, 935 (2013).
- ²²G. A. Ferguson and K. Raghavachari, *J. Chem. Phys.* **125**, 154708 (2006).
- ²³W. Kress and F. W. de Wette, *Surface Phonons* (Springer-Verlag, New York, 1991).
- ²⁴B. Gans, P. A. Knipp, D. D. Koleske, and S. J. Sibener, *Surf. Sci.* **264**, 81 (1992).
- ²⁵D. D. Koleske and S. J. Sibener, *Rev. Sci. Instrum.* **63**, 3852 (1992).
- ²⁶P. Giannozzi, S. Baroni, N. Bonini, M. Calandra, R. Car, C. Cavazzoni, D. Ceresoli, G. L. Chiarotti, M. Cococcioni, I. Dabo, A. Dal Corso, S. de Gironcoli, S. Fabris, G. Fratesi, R. Gebauer, U. Gerstmann, C. Gougoussis, A. Kokalj, M. Lazzeri, L. Martin-Samos, N. Marzari, F. Mauri, R. Mazzarello, S. Paolini, A. Pasquarello, L. Paulatto, C. Sbraccia, S. Scandolo, G. Scalauzero, A. P. Seitsonen, A. Smogunov, P. Umari, and R. M. Wentzcovitch, *J. Phys.: Condens. Matter* **21**, 395502 (2009).
- ²⁷D. Vanderbilt, *Phys. Rev. B* **41**, 7892 (1990).
- ²⁸J. P. Perdew, K. Burke, and M. Ernzerhof, *Phys. Rev. Lett.* **77**, 3865 (1996).
- ²⁹H. J. Monkhorst and J. D. Pack, *Phys. Rev. B* **13**, 5188 (1976).
- ³⁰D. Farías and K.-H. Rieder, *Rep. Prog. Phys.* **61**, 1575 (1998).
- ³¹J. L. Beeby, *J. Phys. C* **4**, L359 (1971).
- ³²J. S. Ha and E. F. Greene, *J. Chem. Phys.* **91**, 7957 (1989).
- ³³K. Ohkuma and K. Nakamura, *J. Phys. C: Solid State Phys.* **12**, L835 (1979).
- ³⁴J. R. Buckland and W. Allison, *J. Chem. Phys.* **112**, 970 (2000).
- ³⁵N. Esbjerg and J. K. Nørskov, *Phys. Rev. Lett.* **45**, 807 (1980).
- ³⁶N. Camillone III, C. E. D. Chidsey, G.-Y. Liu, T. M. Putvinski, and G. Scoles, *J. Chem. Phys.* **94**, 8493 (1991).
- ³⁷C. Kittel, *Introduction to Solid State Physics*, 8th ed. (Wiley, Hoboken, 2004).
- ³⁸G. Nilsson and G. Nelin, *Phys. Rev. B* **3**, 364 (1971).
- ³⁹X. Zeng and H. E. Elsayed-Ali, *Surf. Sci.* **442**, L977 (1999).
- ⁴⁰J. E. Griffiths, *J. Chem. Phys.* **38**, 2879 (1963).

- ⁴¹J. P. Toennies, *J. Vac. Sci. Technol., A* **2**, 1055 (1984).
- ⁴²K. D. Gibson and S. J. Sibener, *Phys. Rev. Lett.* **55**, 1514 (1985).
- ⁴³A. Tamtögl, P. Kraus, M. Mayrhofer-Reinhartsberger, D. Campi, M. Bernasconi, G. Benedek, and W. E. Ernst, *Phys. Rev. B* **87**, 035410 (2013).
- ⁴⁴J. H. Weare, *J. Chem. Phys.* **61**, 2900 (1974).
- ⁴⁵S. Wei and M. Y. Chou, *Phys. Rev. B* **50**, 2221 (1994).
- ⁴⁶X. Han, T. Balgar, and E. Hasselbrink, *J. Chem. Phys.* **130**, 134701 (2009).
- ⁴⁷J. Lobo, D. Farías, E. Hulpke, J. Toennies, and E. Michel, *Phys. Rev. B* **74**, 035303 (2006).
- ⁴⁸A. L. Glebov, J. P. Toennies, S. Vollmer, and G. Benedek, *Europhys. Lett.* **46**, 369 (1999).
- ⁴⁹P. Santini, L. Miglio, G. Benedek, and P. Ruggerone, *Surf. Sci.* **241**, 346 (1991).
- ⁵⁰P. Santini, P. Ruggerone, L. Miglio, and R. B. Doak, *Phys. Rev. B* **46**, 9865 (1992).